Tellus (1990), *42A*, 305–327

The three-dimensional distribution of atmospheric heating during the GWE

By TODD K. SCHAACK, DONALD R. JOHNSON and MING-YING WEI*, *University of Wisconsin–Madison, Space Science and Engineering Center, Madison, Wisconsin 53706, USA*

(Manuscript received 31 May 1988; in final form 15 February 1989)

ABSTRACT

The three-dimensional global distributions of time-averaged atmospheric heating for January, April, July and October 1979 are estimated from the ECMWF GWE Level IIIb data set. Heating rates are calculated through a vertical integration of the isentropic equation of mass continuity. Estimates of the vertical variation of heating are presented in isobaric coordinates through interpolation of the vertical profiles of heating from isentropic to isobaric coordinates. The horizontal distributions of heating and vertical profiles from various climatological regimes of the planetary circulation provide insight into the four-dimensional structure of the thermal forcing of the atmosphere. The large-scale structure of the heating distributions appears spatially and temporally consistent with known features of the global circulation and the seasonal evolution. Major features of the global distributions include the heating in regions of deep moist convection over South America, equatorial Africa, the ITCZ, the Asian monsoon circulation and the oceanic cyclone tracks of the Northern Hemisphere. The primary centers of heating migrate meridionally and zonally with changing seasons. The meridional migration is linked directly with the annual variation of the latitude of maximum incoming solar radiation. The zonal migration is linked with the planetary scale distribution of continents and oceans and the land–sea surface temperature distribution as determined by the surface energy balance and energy transport within the atmosphere itself. Throughout the tropical–subtropical regions, the strongest heating occurs above 600 mb in association with deep convection. Within the primary centers of heating associated with the Asian monsoon circulation, the maximum heating in the vertical profile is near 400 mb. Over the oceanic storm tracks of the Northern Hemisphere, heating occurs through most of the troposphere. The lower tropospheric heating is maximized in January and in that month is significantly stronger than the heating in the middle troposphere. In July there is negligible heating in the lower troposphere. Profiles from the high latitude continental regions such as central Asia and Canada are in close agreement showing cooling through most of the troposphere in winter and modest heating in summer. Profiles from desert regions over the Sahara and western Australia are also in close agreement showing a transition from low level heating to middle and upper level cooling. Cooling occurs throughout the free troposphere in regions of subtropical anticyclonic circulations over the eastern North and South Pacific Oceans.

1. Introduction

Knowledge of the global distribution of heating is important for understanding the earth's planetary circulation. Prior to the Global Weather Experiment (GWE), from December 1978 through November 1979, detailed global analyses of heating were lacking due to the paucity of data over much of the earth. The GWE's enhanced observational system in combination with advances in data assimilation has produced four-dimensional analyses which offer the best description of the global atmosphere to date (National Research Council, 1985). A determi-

* Present affiliation: Meteorology Program, Division of Atmospheric Sciences, National Science Foundation, Washington, DC 20550, USA.

nation of the planetary distribution of heating is now feasible.

Several methods have been used to determine the large-scale heating distributions. One method is to independently estimate the components of radiational, condensational and sensible heating (e.g., Budyko, 1963; Newell et al., 1969, 1974; Otto-Bliesner and Johnson, 1982; Zillman and Johnson, 1985). A second method obtains the net heating from the energy balance required by the First Law of Thermodynamics (e.g., Hantel and Baader, 1978; Geller and Avery, 1978; Lau, 1979; Masuda, 1983). Another method employs the vorticity and thermal balance within quasi-geostrophic theory (e.g., Wiin-Nielsen and Brown, 1962; Brown, 1964). Heating is also calculated from the atmospheric energy budget (Savijärvi, 1988).

For the analysis of global heating distributions from the GWE data, Masuda (1984), Sardeshmukh (1984), Kasahara and Mizzi (1985), Holopainen and Fortelius (1986), Chen and Baker (1986) and Kasahara et al. (1987) employed the thermodynamic equation. Johnson (1985) and Boer (1986) estimated vertically integrated heating from total energy balance, while Wei et al. (1983), Johnson and Wei (1985) and Johnson et al. (1987) computed heating through a vertical integration of the isentropic mass continuity equation. Differences in the methods of calculation, the time periods considered, the assumptions made and the amount of filtering/smoothing employed makes exact comparison of heating distributions from the different investigations difficult. However, overall agreement is apparent in the general features of the heating distributions calculated from the GWE data sets.

The utility of the isentropic method for the estimation of the large-scale heating distributions was demonstrated by Wei et al. (1983) who used the National Meteorological Center (NMC) GWE Level IIIa data to study the vertically averaged and zonally averaged heating distributions during the four seasons of the GWE year. Johnson and Wei (1985) and Johnson et al. (1987) completed similar studies using the European Centre for Medium-range Weather Forecasts (ECMWF) Level IIIb data set. In this paper, the isentropic method is used to estimate the large-scale three-dimensional global distribution of heating for January, April, July and October of 1979 from the ECMWF Level IIIb analyses.

A thorough understanding of the structure and evolution of atmospheric circulation is ultimately linked to obtaining adequate knowledge of the spatial and temporal distribution of atmospheric heat sources and sinks. Previous investigations have demonstrated that in addition to adequately describing the horizontal distributions of heat sources and sinks, a knowledge of the vertical variation of heating is important. The sensitivity of atmospheric response to the vertical variation of heating has been suggested from model results for both tropical (Hartmann et al., 1984) and extratropical (Smagorinsky, 1953; Trenberth, 1983) latitudes. Trenberth (1983) remarks that the results from numerous studies comparing the relative roles of orography and heating in forcing the planetary waves have been mixed due most likely to inadequate specification of the thermal forcing.

The main objective of this paper is to examine the large-scale three-dimensional time-averaged distribution of heating and its temporal evolution as determined from the ECMWF GWE Level IIIb data set. First, global distributions of vertically averaged heating for January, April, July and October 1979 are presented to illustrate the seasonal evolution of the planetary pattern. Next, temporally averaged vertical profiles of heating from various geographical locations demonstrate the seasonal evolution of the vertical structure of atmospheric heating in different climatological regimes. The vertical variation of atmospheric heating and its seasonal evolution are then discussed from a global perspective through presentation of layer-averaged results for each of the four mid-season months of the GWE year. In the analyses, only estimates of the total heating, the sum of all components, can be determined. In the interpretation and discussion of the results, however, frequent statements will be made as to the component (components) of heating that is (are) responsible for the features that are evident in the horizontal and vertical distributions. These statements should be regarded as suggestions and are open to interpretation by the reader.

In the following section, a brief description of the data used in this investigation is given. Section 3 outlines the numerical procedures used

in the calculation of heating. Vertical profiles and global distributions of heating are presented in Section 4, which is followed by a summary.

2. Data

The data used in this study are from the ECMWF GWE Level IIIb data set (Bengtsson et al., 1982). Global distributions of zonal and meridional wind components, temperature, and geopotential height were available on a 1.875° latitude–longitude grid for 15 mandatory pressure levels between 1000 and 10 mb.

Global isentropic analyses were generated on a 3.75° latitude–longitude grid for 0000 and 1200 GMT by linear interpolation of the relevant meterological parameters with p^{κ} ($\kappa = R/c_p$) where p is pressure, R the gas constant for dry air and c_p the specific heat of dry air at constant pressure. In this conversion, surface height and surface values of pressure, temperature and zonal and meridional wind components were needed. Information at the earth's surface was not provided in the ECMWF Level III analyses. Therefore, surface height was obtained through a bi-linear interpolation of the National Meteorological Center's 2.5° latitude–longitude terrain height. Surface pressure was interpolated from the GWE Level III isobaric data by assuming that geopotential varies quadratically with $\ln p$ (Gerrity, 1977). Surface temperature and horizontal wind components were interpolated linearly with $\ln p$ except when surface pressure was greater than 1000 mb. In this case temperature was extrapolated downward from 1000 mb with the standard atmosphere lapse rate of 6.5 K km^{-1}. The temperature fields in the ECMWF Level IIIb data set were from initialized results, whereas the height fields were not (Bengtsson et al., 1982). Because of a preference to conduct the analyses with uninitialized fields, temperature was computed from thickness and layer mean relative humidity. The height information at 150 mb was not utilized due to a possibility of errors at this level (Julian, 1983). A varying vertical resolution in the isentropic domain was adopted; 10°K between 220°K and 380°K, 20°K between 380°K and 500°K, 50°K between 500°K and 550°K followed by 650°K. Pressure on the 650°K level is less than 40 mb over the global domain.

After preliminary calculations, the decision was made to designate 400°K as the top level (θ_T) of the isentropic analyses. The patterns of heating using $\theta_T = 650$°K and $\theta_T = 400$°K are similar over much of the globe. However, inclusion of the data between 400°K and 650°K appears to exaggerate the magnitude of heating in some regions; the largest difference being a doubling of heating rates over portions of eastern Asia in January. This results from rather large values of mass divergence in certain regions above 400°K, particularly over eastern Asia, which are thought to be questionable due to the limited stratospheric data that was available during the initial data assimilation. In each of the four months studied, the time-averaged pressure on the 400°K surface is less than 155 mb over the globe and in January this surface slopes from near 150 mb in extratropical latitudes to near 90 mb in tropical latitudes.

3. Numerical procedure

The isentropic continuity equation (Johnson, 1980) is

$$\frac{\partial}{\partial t_\theta}(\rho J_\theta) + \nabla_\theta \cdot (\rho J_\theta \underset{\sim}{U}) + \frac{\partial}{\partial \theta}(\rho J_\theta \dot{\theta}) = 0, \tag{1}$$

where ρ is density, J_θ is the transformation Jacobian $|\partial z/\partial \theta|$, $\underset{\sim}{U}$ is the horizontal wind velocity and $\dot{\theta} = \mathrm{d}\theta/\mathrm{d}t$. With the hydrostatic relation

$$\rho J_\theta = -\frac{1}{g}\frac{\partial p}{\partial \theta}, \tag{2}$$

the mass within an isentropic layer is determined by the difference in pressure between the upper and lower isentropic levels.

The diabatic mass flux through an isentropic surface is estimated through vertical integration of (1)

$$\rho J_\theta \dot{\theta} = \int_\theta^{\theta_T} \left[\frac{\partial}{\partial t_\theta}(\rho J_\theta) + \nabla_\theta \cdot (\rho J_\theta \underset{\sim}{U})\right] \mathrm{d}\theta, \tag{3}$$

where, in this investigation, the diabatic mass flux is assumed to vanish at the top isentropic surface (θ_T). The heating rate, $\dot{\theta}$, is obtained from the diabatic mass flux according to

$$\dot{\theta} = \rho J_\theta \dot{\theta} / \rho J_\theta. \tag{4}$$

The heating rate $\dot{\theta}$ is equivalent to the rate of specific heat addition, Q, divided by the Exner function

$$\dot{\theta} = Q \Big/ \left(c_p \left(\frac{p}{p_{00}} \right)^{\kappa} \right). \tag{5}$$

Heating rates computed by integration of the right-hand side of (3) with the assimilated data become unrealistic at lower isentropic levels at some locations. This results primarily from inadequacies inherent in assimilating data from sparse irregularly spaced observations and the resulting systematic errors that accumulate through vertical integration of biased estimates of horizontal mass divergence. Although Schmidt and Johnson's (1972) discussion on such errors was directed to the estimation of vertical motion, ω, through the use of the isobaric equation of continuity, the problem encountered in estimating heating profiles from isentropic horizontal divergence is quite similar to the problem encountered estimating ω. In order to remove the vertical integral of this systematic error, a mass-weighted adjustment is applied to the diabatic mass flux. This adjustment is based on the constraint that the sum of the vertically integrated mass tendency and mass divergence must reduce to a boundary value for diabatic mass flux through isentropic surfaces at the earth's surface. The adjusted diabatic mass flux is obtained according to

$$(\rho J_\theta \dot{\theta})' = \int_{\theta}^{\theta_T} \left[\frac{\partial}{\partial t_\theta} (\rho J_\theta) + \nabla_\theta \cdot (\rho J_\theta \underset{\sim}{U}) - \rho J_\theta \hat{\delta} \right] \mathrm{d}\theta, \tag{6}$$

where $(\ )'$ denotes the adjusted value of the diabatic mass flux at an isentropic level while $\hat{\delta}$ represents an error per unit mass within the atmospheric column. See Appendix for details of the adjustment employed.

The three-dimensional global distribution of heating is calculated for 0000 and 1200 GMT of each day of January, April, July and October 1979. The vertical profile of heating at each grid point is estimated from the adjusted diabatic mass flux in (6). The mass tendency in (6) is evaluated as a 24-h centered difference while the divergence is calculated from data at the central time period.

The mass-weighted temporally and vertically averaged heating rates discussed in the following section are estimated from

$$\hat{\dot{\theta}}^{\theta,t} = \int_{\theta_s}^{\theta_T} \int_{t_1}^{t_2} \rho J_\theta \dot{\theta} \, \mathrm{d}t \, \mathrm{d}\theta \Big/ \int_{\theta_s}^{\theta_T} \int_{t_1}^{t_2} \rho J_\theta \, \mathrm{d}t \, \mathrm{d}\theta, \tag{7}$$

where t_1 and t_2 are the beginning and end of the time-averaging period, respectively. $\theta_s(\lambda, \phi, t)$ is the potential temperature at the earth's surface, λ is longitude and ϕ is latitude.

Although the heating rates were calculated by integration of the isentropic mass continuity equation, the vertical structure of heating is presented in isobaric coordinates. The isobaric heating rates were obtained by vertically interpolating the isentropic profiles of heating at individual grid points to isobaric levels at 50 mb increments between 150 mb and the earth's surface assuming a linear variation with p^{κ}. This interpolation was carried out at each time period and monthly isobaric averages were calculated from twice daily results.

Vertical profiles of time-averaged heating for individual grid points are discussed in Subsection 4.2. Global distributions of time- and layer-averaged heating for four isobaric layers between the surface and 200 mb are shown in Subsection 4.3. The global distributions are expressed as heating per unit mass in order to properly account for the condition that the earth's surface bounds the lowest layer and also occasionally bounds the second lowest layer in regions of elevated orography such as the Tibetan Plateau.

Johnson et al. (1987) presented estimates of the large-scale heating rates for corresponding isobaric layers for January and July 1979. The method of calculation utilized in the present study is the same as in their investigation except for the following differences. The heating rates in the present study were calculated, and interpolated from isentropic to isobaric coordinates at each time period of the month considered and subsequently time-averaged in isobaric coordinates. The isobaric heating rates in Johnson et al. (1987) were obtained through interpolation of the monthly averaged heating rates on isentropic levels to isobaric levels assuming a linear variation with $(\bar{p}')^{\kappa}$. Since the pressure on isentropic surfaces fluctuates with time, interpolation utilizing time-averaged fields may not yield completely

representative vertical profiles of time-averaged heating in isobaric coordinates.

Two computational problems encountered in estimating the vertical profile of heating near the earth's surface with the isentropic method are: (1) the partitioning of the lower boundary value of diabatic mass flux (see eq. (A3) in the Appendix), and (2) estimation of static stability (ρJ_θ is a measure of inverse static stability, see eq. (2)) in transient baroclinic regions where several grid volumes in the vertical intersect the surface of the earth during the time averaging interval. The computational methods used in these situations in the present study differs from that of Johnson et al. (1987). The different methods only affect results near the earth's surface and the net effect is small over much of the globe. In highly baroclinic regions, the estimates in the lower levels of the present study tend to be reduced in magnitude compared to Johnson et al. (1987).

Comparison of corresponding horizontal distributions of layer-averaged heating from the present study and Johnson et al. (1987) shows the only significant differences occur over the oceanic cyclone tracks of the Northern Hemisphere in January. Although there is uncertainty, it is felt the distributions in the present study offer improved estimates of the isobaric temporally averaged heating in these regions.

The global analyses presented in this paper have been filtered in order to emphasize large-scale features and eliminate noise. First, zonal harmonics with wavelengths less than 4000 km are removed through truncation of one dimensional Fourier transforms (Wei et al., 1983). Spatial smoothing is applied in the north–south direction through a combination of four passes of a low pass (2, 3, 2) filter and one pass of an inverse (−1, 5, −1) filter. Fig. 1 shows the response of the meridional smoothing at different wavelengths. The vertical profiles of heating in Fig. 4 were extracted from horizontal distributions of temporally averaged heating on isobaric levels that have been filtered as described above.

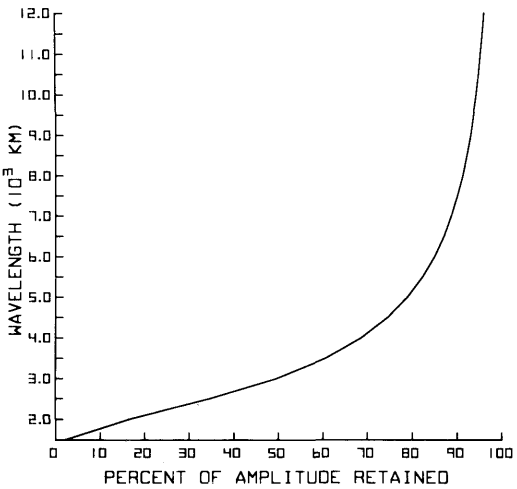

Fig. 1. Response of the meridional smoothing composed of four passes of a low-pass (2, 3, 2) filter and one-pass of an inverse (−1, 5, −1) filter.

4. Results

Monthly averaged heating distributions are calculated for January, April, July and October 1979. In the discussion that follows, emphasis is placed on the vertical structure of heating. In order to facilitate discussion and provide a background for the temporal changes in the vertical structure, horizontal distributions of vertically averaged heating will be described first. Vertical profiles of heating at selected locations are then presented, followed by horizontal distributions of layer-averaged heating for four isobaric layers between the surface and 200 mb.

4.1. Vertically averaged heating

Global distributions of mass-weighted vertically averaged heating for January, April, July and October 1979 are shown in Fig. 2. For the most part the heating distributions are in excellent agreement with physical considerations.

In January (Fig. 2A) cooling of 0.5 to 1.5°K day^{-1} occurs over most of the Northern Hemisphere's continental and polar regions, while heating is present over the oceans. Strong heating with maxima in excess of 1.5°K day^{-1} occurs off the east coasts of Japan and the United States. The axes of strongest heating in these regions are oriented along the oceanic cyclone tracks over the Kuroshio Current and the Gulf Stream. In the tropics, heating occurs in regions of active convection along the Intertropical Convergence Zone (ITCZ) extending from South America across the Atlantic, Africa, the Indian

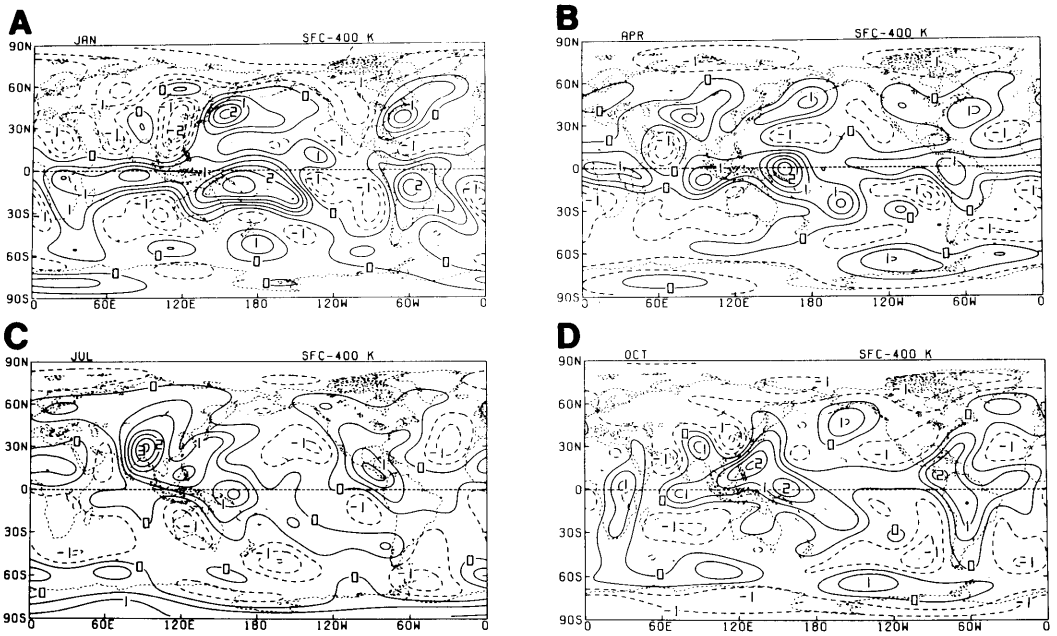

Fig. 2. Mass-weighted temporally and vertically averaged heating rates (°K day^{-1}) computed from the ECMWF GWE Level IIIb analyses for (A) January, (B) April, (C) July, and (D) October 1979. Filtered to emphasize wavelengths greater than 4000 km. Contour interval is 0.5°K day^{-1}.

Ocean and into the mid-Pacific. Well defined cooling maxima exceeding 1.0°K day^{-1} are located in regions of oceanic anticyclonic circulations west of Australia, South America and southern Africa.

A heating maximum greater than 2.5°K day^{-1} occurs over the equatorial western Pacific associated with moist convection of the winter Asian monsoon. The regions of maximum heating over the equatorial western Pacific and over the eastern Indian Ocean near 90°E are the principal ascending branches of the Asian winter monsoon during the GWE year (Sumi and Murakami, 1981). Sumi and Murakami noted that this distribution differs from the circulation in previous years in which the ascending branch of the winter monsoon is centered over Indonesia. Heating extends from the maximum over the equatorial western Pacific southeastward into the South Pacific along the South Pacific Convergence Zone (SPCZ). Throughout the text, Asian monsoon refers to the seasonally varying regimes of the planetary circulation which extend in latitude from the northern reaches of Eurasia to the southern oceans and in longitude from across Africa to the west and the Pacific Ocean to the east (Webster et al., 1977).

The distribution of heating/cooling in tropical latitudes is in good agreement with the time-averaged distribution of outgoing longwave radiation for the 25-day period ending 31 January 1979 shown by Gruber et al. (1986). The global heating distribution also agrees very well with the distributions of monthly averaged cloud fraction and cloudtop pressure for Janaury 1979 shown by Susskind and Kalnay (1985). These satellite-derived cloud parameters substantiate most of the major features of the heating distribution in Fig. 2A, such as the oceanic cyclone tracks of the North Atlantic and North Pacific, the ITCZ and the SPCZ. The cloudtop pressure in Fig. 6 of Susskind and Kalnay distinguishes the deep convection of tropical regions from the low level stratiform clouds frequently occurring to the west of continents in the Southern Hemisphere. The cooling over northern Africa, between 80° and 140°W in the topics and over nearly all longitudes of the Northern Hemisphere subtropics, except between 110° and 150°W, corresponds to regions of low percentage cloud cover in January 1979.

Two features of the January heating distribution where the interpretation is not as clear are the heating over the eastern Soviet Union near 60°N and the heating centered over the Tibetan Plateau. A tabulation of cyclone activity during January 1979 (L. Whittaker, personal communication) identifies a region with relatively high cyclone frequency extending from over central Asia to the Pacific Ocean centered on 55°N. The heating over the eastern Soviet Union in Fig. 2A lies along this axis downstream of the maximum frequency and may reflect latent heating within these disturbances. However, Fig. 6 shows the major contribution to heating in this region occurs above 400 mb. The heating distribution calculated using 650°K as the top of the isentropic data set (not shown) indicates strong heating in the 400–650°K layer in this region. This vertical distribution, with the elevated level of heating, suggests that the heating in this region may be erroneous. Results for January 1979 computed from NMC Level IIIa data by Johnson, Townsend and Wei (1985) also show strong heating in this region. The vertically integrated heating for February 1979 calculated from both ECMWF and Goddard Laboratory for Atmospheres (GLA) GWE data by Holopainen and Fortelius (1986) also indicate strong heating in this region. They question the validity of heating in this region during February. The results from the different GWE data sets indicate this feature is not specific to the ECMWF assimilation system.

The net heating over the Tibetan Plateau during January does not agree with results from earlier investigations which indicate the region above the Plateau to be a wintertime heat sink (Staff Members of Academia Sinica, 1958; Yeh and Gao, 1979). In a recent investigation, Kasahara et al. (1987) calculated time-averaged heating rates for the period 27 January to 10 February 1979 using GWE Level IIIb data from both ECMWF and the Geophysical Fluid Dynamics Laboratory (GFDL). The ECMWF results showed a heat source over the Tibetan Plateau while the GFDL results indicated strong cooling in the region. Kasahara et al. state that it is likely that ECMWF results are unrealistic. However, the high percentage cloud cover and low cloudtop pressure heights over the Plateau in January 1979 shown by Susskind and Kalnay (1985) suggest the possibility of an energy source from latent heat release. Heating over the Plateau also appears in the heating distribution computed from the NMC Level IIIa data (Wei et al., 1983). This issue remains unresolved.

In April (Fig. 2B), the heating distribution indicates an ITCZ centered on or near the equator completely circumscribing the globe. The maximum heating, exceeding 2.5°K day^{-1}, is shifted north and west from the January position and is centered on the equator near 160°E. An axis of heating extends from this area into the South Pacific along the SPCZ. Other relative maxima in the tropics occur over equatorial Africa, over the equator near 100°E and over equatorial South America.

In the Northern Hemisphere, the heating distributions over the western oceans and the orientation of the axes of strongest heating are in good agreement with climatological cyclone tracks of April (Whittaker and Horn, 1982). The heating over much of the continental regions south of 60°N in the Northern Hemisphere likely reflects sensible heat flux from the earth to the atmosphere from increased solar insolation over January and increased latent heat release through deep convection over continental regions in the spring season. The heating over the Tibetan Plateau and surrounding area agrees qualitatively with results by Yeh and Gao (1979).

In July (Fig. 2C), the dominant planetary feature is the large area of heating centered over southeast Asia and the equatorial western Pacific associated with the summer Asian monsoon. The maximum heating, exceeding 3.0°K day^{-1}, lies to the north of the Bay of Bengal over the foothills of the Himalayas. An axis of strong heating extends southeastward to the equatorial western Pacific and into the South Pacific along the SPCZ. A second axis of heating, nearly perpendicular to the first, lies just off the east coast of Asia. The distribution of heating over southeast Asia and the East Indies and the location of the maximum heating north of the Bay of Bengal agrees well with the distribution of the intensity index of convection (I_c) for July 1979 shown by Murakami (1983). The intensity index of convection is derived from satellite infrared irradiance data and provides an estimate of the fraction of convective clouds within a region that extend above 400 mb. Monthly averaged distributions

of this index identify regions with frequent occurrence of deep convection which in turn should correspond to regions of atmospheric heating due to latent heat release.

In the Northern Hemisphere, heating dominates continental regions equatorward of 70°N, while cooling exists over the eastern oceans. Two axes of heating are evident over North America. One lies along the continental divide and the other extends along the eastern coast. The maximum heating in the Western Hemisphere, centered over Central America, is associated with deep moist convection.

Well defined cooling maxima with rates exceeding 1.0°K day^{-1} are located over the eastern oceans of the Northern Hemisphere within subtropical anticyclonic circulations. Cooling generally prevails in Southern Hemisphere subtropical and extratropical latitudes. The heating between 50–60°S in the region south of Africa and in the Indian Ocean corresponds with a storm track of the Southern Hemisphere GWE winter season (Physick, 1981). The heating over most of Antarctica appears questionable. Results from the NMC Level IIIa data (Wei et al., 1983) indicate cooling over Antarctica in the winter season.

In October (Fig. 2D), the maximum heating within the Asian monsoon is located southeast of the July position with rates exceeding 2.0°K day^{-1} just to the east of the Philippines and over the equator near 160°E. Cooling over northern polar regions during July expands to cover nearly all of the Northern Hemisphere continental regions in October. The increase in heating over the Gulf of Alaska and southeast of Greenland compared to July is a reflection of the increase in intensity and frequency of extratropical cyclones in these regions (Whittaker and Horn, 1982).

In the Southern Hemisphere, heating extends over all of Africa and South America showing a seasonal transition from the wintertime cooling in these regions during July to the summertime heating maximum in January. The cooling to the west of southern Africa, Australia and Chile corresponds with the location of the Southern Hemisphere's anticyclonic circulations. Cooling greater than 0.5°K day^{-1} spans most of Antarctica.

The major features of the heating distributions just discussed appear realistic. Most features are associated with atmospheric circulations in which either latent or sensible heating persists or the lack of convection and cloudiness permits radiational cooling to dominate. The heating distributions also show realistic seasonal variations. For example, the heating within the ITCZ and Asian monsoon follows the seasonal march of incoming solar radiation from one hemisphere to the other. The contrasts associated with the distribution of land and oceans are also evident with heating over continents and cooling over oceans in the summer and the opposite distribution in the winter season of both hemispheres. This contrast is particularly pronounced in the Northern Hemisphere.

4.2. Vertical profiles of heating

The net heating distributions presented herein represent the sum of sources and sinks of energy by radiation and latent and sensible heat addition. The method of calculation in this study does not provide insight into the relative importance of the individual components. However, since sensible heating is strongest within the planetary boundary layer, while latent heating normally is maximized in the middle and upper troposphere, through inference, the vertical distribution of heating as well as seasonal and geographical variations provides qualitative information on the contribution by individual components.

Since heating rates were computed by integration of the isentropic mass continuity equation, the vertical structure of heating from these results is most readily displayed in isentropic coordinates. However, with the majority of work in atmospheric science being performed in isobaric coordinates, the profiles of heating are presented as a function of pressure for ready application and comparison with other results. As discussed in Section 3, isobaric heating rates at 50 mb increments between 150 mb and the earth's surface were obtained twice daily through interpolation from isentropic coordinates assuming a linear variation with p^{κ}. With interpolation being carried out at each time period and subsequent temporal averaging conducted in isobaric coordinates, the results are in fact temporally averaged isobaric distributions of heating. From the global isobaric analyses which were filtered as described in Section 3, vertical

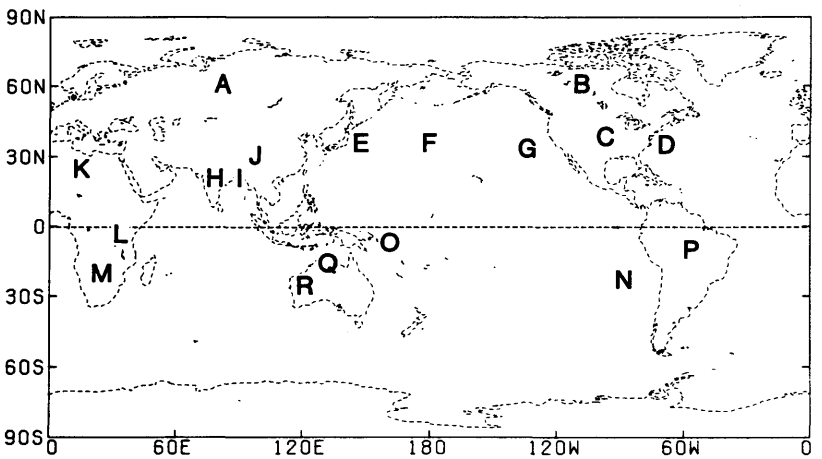

Fig. 3. Geographical locations of the vertical profiles of heating shown in Fig. 4.

profiles of time-averaged heating for January, April, July and October 1979 at eighteen grid points (Fig. 3) were selected to demonstrate distinct regimes of the planetary circulation. The agreement of the following profiles with climatological and physical considerations is, for the most part, representative of the agreement at other arbitrary geographical locations. No screening was made during the analysis to locate profiles which optimally portray climatological features seasonally or annually.

Heating profiles from three continental regions: the central Soviet Union, Canada and the United States are shown in Figs. 4A, 4B and 4C, respectively. The profiles over the Soviet Union and Canada are similar in each month, while all three locations have similar vertical distributions in January and October. In January, when high pressure systems persist over the continental land masses of the Northern Hemisphere, cooling between 1.0 and 2.0°K day^{-1} is indicated through most of the troposphere at all three locations. This magnitude reasonably compares with the zonal mean radiative cooling rate of 0.5 to 1.5°K day^{-1} for the winter season in middle latitudes of the Northern Hemisphere shown by Dopplick (1972). The July profiles over the Soviet Union and Canada indicate weak heating through most of the troposphere suggesting that sensible heating in low layers and heating within summertime convection offset the heat loss by radiation. The profiles over the central United States show relatively strong middle and upper tropospheric heating in both April and July. The profile in Fig. 4C lies along a major cyclone track of April (Whittaker and Horn, 1982). Thus, the upper level heating in April presumably results in part from latent heat release within cyclones and springtime convection. The upper tropospheric heating in July likely results from summertime convection over the Great Plains.

Fig. 4D shows profiles for a point over the Gulf Stream in the western Atlantic. Heating is indicated through most of the troposphere in all four months. The January, April and October profiles show significant lower level heating that must be largely attributed to sensible heating over the Gulf Stream; the heating is by far the strongest in January when the temperature difference between the ocean and overlying air of continental origin is large. The heating in the middle and upper troposphere in these three months must result from latent heating in cyclonic disturbances which traverse the region. The minimal low level heating in July reflects the minimal temperature contrast between the ocean and atmosphere in that month. The mid-tropospheric heating in July, which exceeds 1.0°K day^{-1} between 650 and 400 mb, is likely a reflection of summertime convective activity within cyclonic disturbances.

The grid point represented in Fig. 4E lies to the east of Japan over the Kuroshio Current. The

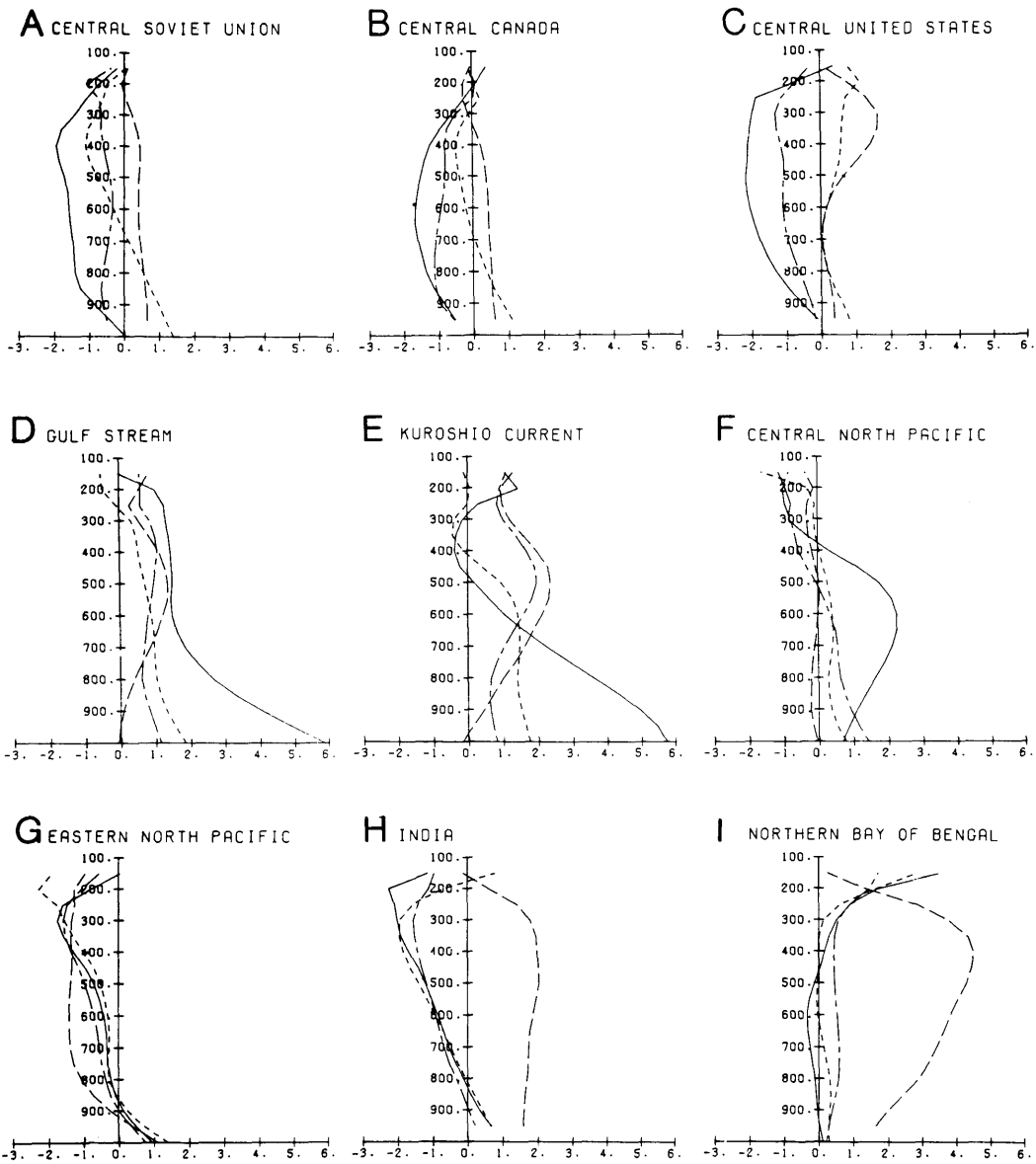

Fig. 4. Vertical profiles of time-averaged heating (°K day^{-1}) for January (——), April (– – –), July (— — —), and October (— — —) 1979. See Fig. 3 for geographical locations.

profiles in this region are, to a large degree, similar to the profiles for corresponding months over the Gulf Stream (Fig. 4D) owing to the similar geographical setting. However, differences are noted. The January profile in both regions shows strong low and middle level heating which must result from a combination of sensible heating at the lower boundary and latent heating within baroclinic disturbances. While the profile over the Gulf Stream shows a nearly constant heating rate of 1.7°K day^{-1} above 700 mb, the profile over the Kuroshio Current

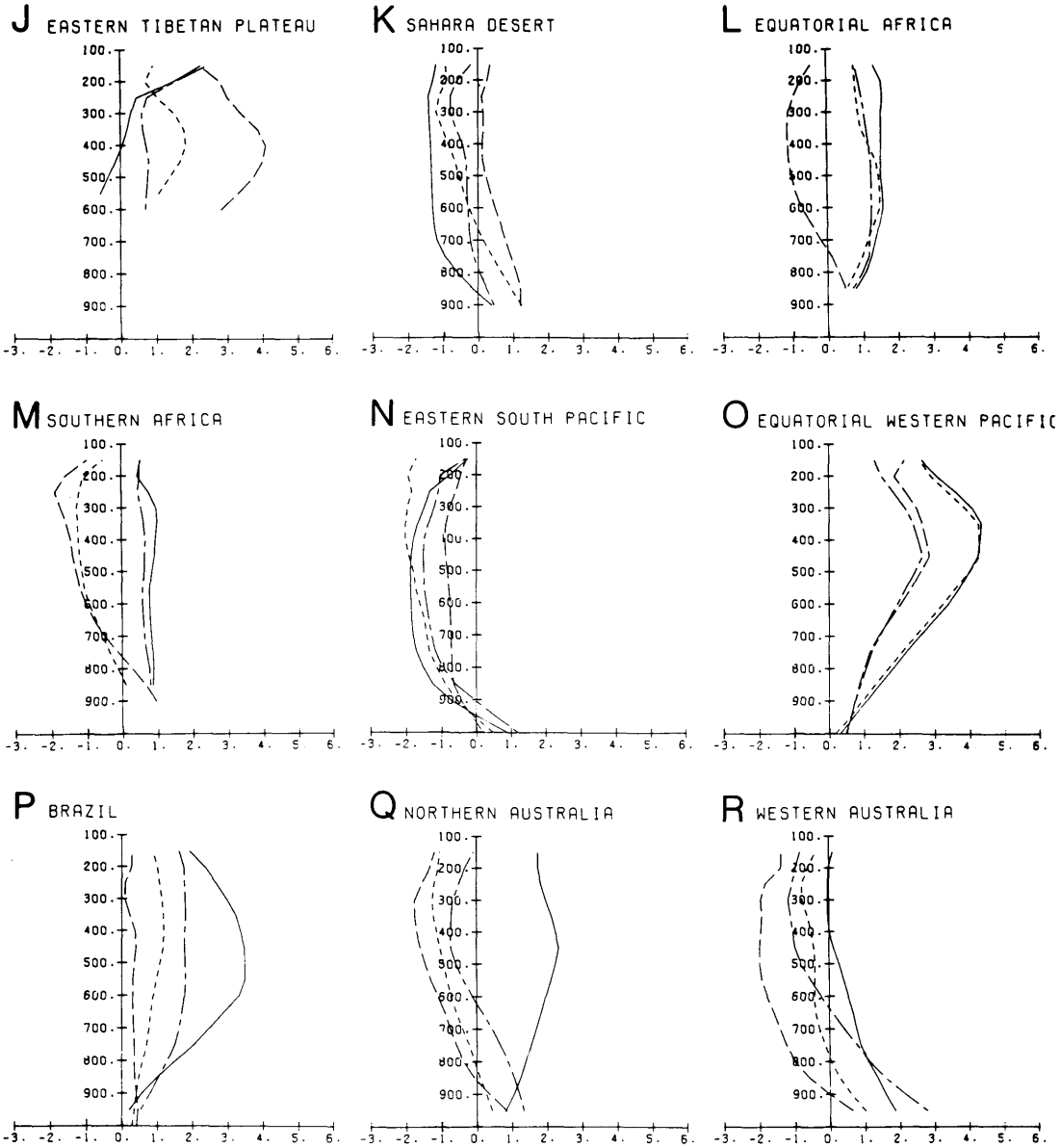

Fig. 4 (continued)

exhibits cooling between 500 and 300 mb. Previous investigations have indicated that many of the cyclones in the vicinity of the Asian coast are shallow features confined to the lower layers of the troposphere (Chen et al., 1985; Nitta and Yamamoto, 1974). Climatologically, little cyclogenetic activity occurs upstream over the Asian continent in January (Whittaker and Horn, 1982), while the cyclones that do form over land are frequently shallow lows (Chen and Dell'Osso, 1987) that never reach the intensity of their counterparts occurring over the North American

continent (Boyle and Chen, 1987). A tabulation of cyclones during January 1979 (L. Whittaker, personal communication) shows little activity over Asia south of 50°N. Since the grid point under consideration lies near the upstream edge of the western Pacific cyclogenetic region, few strongly developed cyclones traversed this region and therefore the net heating was primarily confined to the lower half of the troposphere. The heating above 250 mb in this profile appears questionable as well as in several other profiles that are discussed later. Because of the relatively large variation of ρJ_θ near the tropopause and uncertainty of information in the stratosphere heating estimates in the uppermost levels are less reliable. Comparison of the July and October profiles between Figs. 4D and E shows similar vertical structure, although the heating over the western North Pacific is stronger in the middle troposphere.

Fig. 4F represents a grid point that lies downstream from Fig. 4E in the mid-Pacific oceanic cyclone track for January. The January profile, with a maximum greater than 2.0°K day^{-1} between 700 and 500 mb, is indicative of latent heating within oceanic cyclones that form over the western Pacific and develop during movement to the mid-Pacific. The low level heating is substantially weaker than in Fig. 4E, since the atmosphere within the boundary layer will have undergone substantial modification prior to reaching the mid-Pacific.

Further information on the time-averaged heating over the oceanic storm tracks of the Northern Hemisphere is provided by Fig. 5 which shows vertical cross sections along the axes of strongest heating in these regions. The cross section over the North Pacific (Fig. 5A) lies along 40°N and extends from 110°E over Asia to 120°W in the eastern Pacific. Cooling over the Asian continent switches to heating through the depth of the troposphere near Japan at about 140°E. The strongest heating associated with the modification of polar outbreaks moving southeastward is confined to lower levels just to the east of Japan. The axis of strongest heating tilts eastward with height and reflects the transition from strong sensible heating of the lower troposphere and latent heating within relatively shallow systems over the Kuroshio Current at the western boundary of the North Pacific to latent heating in the middle troposphere over the mid-Pacific as the cyclones develop vertically downstream.

The cross section over the North Atlantic (Fig. 5B) extends from 20°N, 92°W to 70°N, 13°W and lies approximately along a straight line between Florida and Iceland. The strong low-level heating along the entire path reflects heating as polar continental air masses flow southeastward over the warm ocean currents adjacent to North America and Greenland. The strongest heating is located between 30°N and 40°N with the heating in both the upper and lower troposphere being maximized in this region. As noted earlier, the heating distribution in the uppermost levels is questionable.

The vertical structure of heating in Fig. 5A differs from the time-averaged January distribution for a 5-year period shown by Geller and Avery (1978). Their results, showing the Northern Hemispheric distributions at 900 and 500 mb, indicate substantially stronger heating in the middle troposphere than at lower levels over the western North Pacific. This contrasts the results in the present study which indicate the opposite distribution. Over the western North Atlantic (Fig. 5B), both studies indicate stronger heating in the lower troposphere than in the middle troposphere.

Fig. 4G represents a point over the eastern subtropical North pacific that lies within subtropical anticyclonic circulations. Cooling rates between 0.5 and 1.5°K day^{-1} occur through much of the troposphere in all four months. The January, April and October profiles are very similar. In July, when the subtropical high pressure system of the North Pacific is near maximum intensity, the profile shows stronger cooling of the lower and middle troposphere than in the other three months.

Fig. 4H over central India illustrates the seasonality of the Indian monsoon. In July, heating near 2.0°K day^{-1} occurs through most of the troposphere. In the other three months cooling, with a maximum in the upper troposphere, prevails above 800 mb. Sensible heating over the subtropical landmass offsets the radiational cooling in the low troposphere.

Figs. 4I and 4J show profiles from the region of maximum heating of the Asian summer monsoon. The July profile in Fig. 4I, for a point over

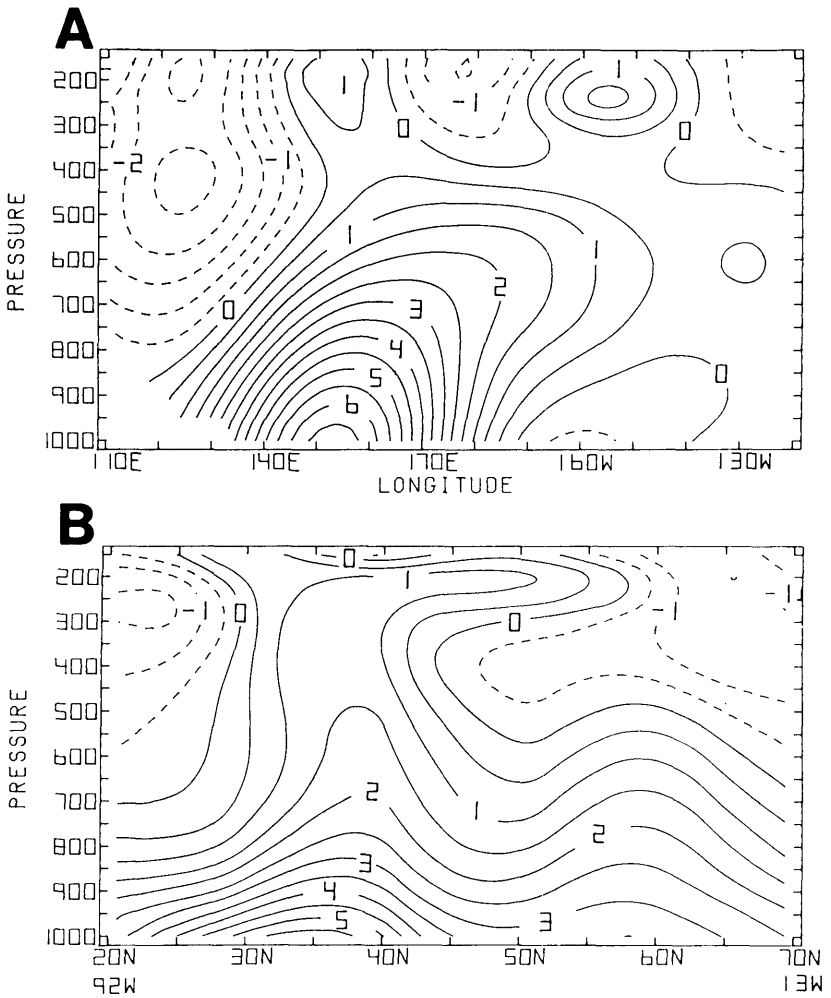

Fig. 5. Cross sections of heating (°K day^{-1}) along the storm tracks of the (A) North Pacific and (B) North Atlantic for January 1979. (A) lies along 40° N from 110° E to 120° W. (B) lies approximately along a straight line between 20° N, 92° W and 70° N, 13° W. Contour interval is 0.5 °K day^{-1}.

the northern Bay of Bengal, has very strong heating through most of the troposphere. This heating, which must be associated primarily with latent heat release in the deep convection of the summer monsoon, has a maximum intensity of 4.5 °K day^{-1} at 400 mb. This July profile compares favorably with heating estimates by Nitta (1983) and Luo and Yanai (1984) who utilized GWE Level IIb data. Nitta (1983) estimated profiles of time-averaged heating at 0000 and at 1200 GMT for June to August 1979 for a region that includes the southeastern Tibetan Plateau, the southeastern foothills of the Plateau and the Assam region. Luo and Yanai (1984) estimated time-averaged profiles of heating for the 40-day period from late May to early July 1979 for a region that includes the Assam Plain, Bangladesh and part of northeast India. All three profiles show similar vertical structure with maximum heating occurring between 400 and 500 mb. In the July profile of Fig. 4I, the heating maximum is near 4.5 °K day^{-1}. With the heating expressed in terms of $\dot{\theta}$ using (5), the maximum heating from the average of Nitta's 0000 and 1200 GMT

profiles is near 4.5°K day^{-1}. The profile from Luo and Yanai with a maximum near 6.5°K day^{-1} shows stronger heating between 300 and 600 mb than the other two profiles. The similarity between results from the Level II and Level III data sets suggest that the ECMWF assimilation model accurately depicted the atmospheric structure at least in regions where data coverage was relatively dense.

Fig. 4J represents a point over the east central Tibetan Plateau. It is interesting to note the similar vertical structures, although with differing magnitudes, of the January and October profiles and the April and July profiles. The strong heating above 250 mb in January and October is questionable. In July, relatively strong heating greater than 2.5°K day^{-1} is indicated in the lowest layers, while the maximum heating of 4.5°K day^{-1} occurs at 400 mb. This profile agrees reasonably well with results by Nitta (1983) and Luo and Yanai (1984) for the corresponding region, although the agreement among the three profiles is less than in results discussed for the previous figure. Nitta and Luo and Yanai found that both sensible and latent heating contribute to the total heating through much of the troposphere over the east central Plateau.

The next three figures portray distributions from Africa; Fig. 4K the Sahara Desert, Fig. 4L the equatorial region and Fig. 4M the southern region. Since the Sahara receives little rainfall, radiational cooling and sensible heating are the dominant heating components. Indeed, sensible heating is reflected in the low troposphere in all four months (Fig. 4K). The strongest low level heating occurs in April and July and the weakest in January and October. In July, significant heating extends from the surface into the middle troposphere. Over a strongly heated surface significant sensible heating of the lower and middle troposphere occurs by dry turbulent convection. Nitta (1983) and Luo and Yanai (1984) have suggested that a portion of middle tropospheric heating over the Tibetan Plateau in the summer is due to upward sensible heat flux associated with dry convection. In the other three months, low level heating switches to cooling within the lower troposphere.

According to the global precipitation climatology compiled by Jaeger (1976), equatorial Africa (Fig. 4L) receives substantial amounts of rainfall in January, April and October. In the profiles for January, April and October, the heating above 800 mb which ranges between 1.0 and 2.0°K day^{-1} is indicative of latent heat release. In July, Jaeger's precipitation climatology shows that the region of maximum rainfall over central Africa lies north of the equator and exhibits a sharp cutoff south of the equator. Hence, in July this profile lies within a region of suppressed convection and radiational cooling likely dominates above 700 mb.

Fig. 4M shows profiles over the highlands of south central Africa. In January and October, the profiles indicate that latent heating dominates over radiational cooling. In April and July, the cooling above 800 mb suggests relatively little moist convection during these months. The climatological distributions of Jaeger (1976) show moderate rainfall in this region in January with lesser amounts in April and October and dry conditions in July. The January and July profiles appear consistent with the climatological precipitation estimates. However, the April and October profiles are more difficult to substantiate, since the climatological precipitation estimates in these months are relatively small and year to year variation in this arid region could change these profiles from heating to cooling or vice versa.

The profiles from the eastern subtropical South Pacific west of Chile shown in Fig. 4N, where anticyclonic circulation dominates in all four months, are similar to those over the eastern subtropical North Pacific (Fig. 4G). Cooling occurs through the depth of the troposphere in each month. The cooling in the lower and middle troposphere is somewhat stronger over the South than the North Pacific in every month except July.

The profiles in O from Fig. 4 are from the equatorial western Pacific, the region of maximum heating of the winter Asian monsoon. The shape of the profiles is remarkably similar in all four months. In January and April, heating increases from near zero at the surface to a maximum of 4.5°K day^{-1} at 350 mb. The heating during July and October is less than in January and April, while the level of maximum heating in these months has lowered to 450 mb. The level of maximum heating in these profiles corresponds

with the level of maximum heating within mature tropical cloud systems (Houze, 1982; Johnson and Young, 1983) and indicates the convection in the monsoon region occurs primarily through mesoscale organization. It should be noted, however, that in terms of instantaneous values of $\dot{\theta}$ the magnitude of the maximum heating estimated exclusively for tropical cloud clusters by Houze (1982) is approximately 35°K day^{-1}, while the estimate of maximum heating within mesoscale anvils by Johnson and Young (1983) is near 20°K day^{-1}. The large differences in magnitude are not surprising since the results of Houze, and Johnson and Young are exclusively for active disturbances while the present results are monthly averaged grid point values and have been filtered as discussed in Section 3.

The profiles in O from Fig. 4 are similar in vertical structure to profiles of heating derived from Q_1 budget studies over the Marshall Islands in the equatorial western Pacific by Yanai et al. (1973) and Reed and Recker (1971), and over the SPCZ by Miller and Vincent (1987). Yanai et al. (1973) utilized data collected during the period 15 April to 22 July 1956. Reed and Recker's (1971) results were derived from a composite of 18 disturbances during July–September of 1967. The results of Miller and Vincent (1987) are for 10–18 January 1979, a period of persistent convective activity in the SPCZ. The above three studies show maxima of heating between 500 and 400 mb. The maximum heating in the three studies is 1.5 to 2.0 times stronger than in the present study. The results of Reed and Recker and Miller and Vincent estimate heating within regions of active disturbances and would be expected to show stronger heating than in the monthly-averaged profiles of the present results. The agreement of the present results with the above studies appears reasonable considering the differences in the analysis techniques, including filtering, and the time periods studied.

The January profile in Fig. 4P for central Brazil shows strong middle and upper tropospheric heating. Heating over 3.0°K day^{-1} occurs between 650 and 300 mb. The heating is weaker in October and April and weakest in July. By inference, the seasonal variation in the magnitude of the heating in these results is in qualitative agreement with the seasonal variation of the cloud distributions in GOES imagery and with the outgoing longwave radiation shown by Heddinghaus and Krueger (1981) for the period of June 1974 to February 1978.

The last two profiles contrast climatic features of regions in north central (Fig. 4Q) and western (Fig. 4R) Australia. Low level heating is indicated in each of the four months over north central Australia. The January profile which shows heating throughout the troposphere is indicative of latent heating associated with the Australian monsoon (Davidson, 1984). In the other three months, radiational cooling apparently dominates to produce net cooling of the middle and upper troposphere. The profiles in this study are consistent with Jaeger's (1976) precipitation climatology which indicates substantial precipitation over northern Australia in January and relatively dry conditions in the other three months.

Lacking substantial amounts of rainfall, cooling generally exists through most of the troposphere over arid western Australia (Fig. 4R) except during January and October when heating extends into middle troposphere. The western Australia profile is located over desert, therefore the indicated heating is likely due to sensible heating. Monthly mean surface temperatures near 310°K were present over western Australia in January 1979 (Susskind and Kalnay, 1985), suggesting sensible heating through a deep layer. The April, July and October profiles in Figs. 4Q and 4R are similar. However, the January profiles are different probably due to a lack of monsoonal rainfall in western Australia.

Similarities in the profiles for corresponding seasons between the desert regions of western Australia (Fig. 4R) and the Sahara (Fig. 4K) are worth noting. In both regions, tropospheric cooling is maximized during the winter month, while heating extends through much of the lower and mid troposphere in the summer month. The corresponding intermediate seasons also show similar vertical structures. The maximum heating in the low levels is nearly twice as strong over western Australia as over the Sahara in corresponding seasons. The similarities between profiles of corresponding seasons of these two regions again demonstrate a consistency in the ECMWF analyses.

4.3. *Isobaric layer-averaged heating*

In Subsection 4.2, the vertical profiles of heating at selected locations were discussed in detail. Presentation of profiles from all potential regions of interest is not feasible. Thus, for illustrating the spatial and temporal continuity of the vertical variation of heating, global distributions averaged within four isobaric layers between the surface and 200 mb are now presented. Figs. 6 through 9 show layer-averaged heating distributions for January, April, July and October, 1979, respectively, in the following sequence, (A) surface to 800 mb, (B) 800–600 mb, (C) 600–400 mb, and (D) 400–200 mb. As discussed in Section 3, the distributions represent the heating per unit mass within the isobaric layer. Variations in the mass of the layer due to spatial variability of time-averaged surface pressure are accounted for (even above 800 mb).

In January, the dominant features in the sfc–800 mb layer (Fig. 6A) are the strong heating maxima over the western oceans of the Northern Hemisphere. This heating is undoubtedly associated with sensible heat flux from the ocean to the atmosphere during outbreaks of cold continental air over the warm Kuroshio Current and the Gulf Stream and the general migration of polar anticyclones into the subtropics. Heating greater than 1.0°K day^{-1} spans a large portion of the western North Pacific between 15°N and 60°N. A maximum of 5.5°K day^{-1} occurs to the east of Japan. In the North Atlantic, heating in excess of 4.0°K day^{-1} occurs off the east coast of the United States. A second maxima of 2.5°K day^{-1} is located southeast of Greenland. Heating in excess of 1.0°K day^{-1} spans the western North Atlantic from 10°N to 75°N. The heating which extends poleward to the north and east of Scandinavia coincides with the northern limits of the North Atlantic Current.

Strong heating, oriented along the oceanic cyclone tracks over the Kuroshio and Gulf Stream Currents, is present in the upper three layers (Figs. 6B–D) over the western North Pacific and North Atlantic. As illustrated in Fig. 5, over the North Pacific the maximum heating shifts from the sfc–800 mb layer over the western

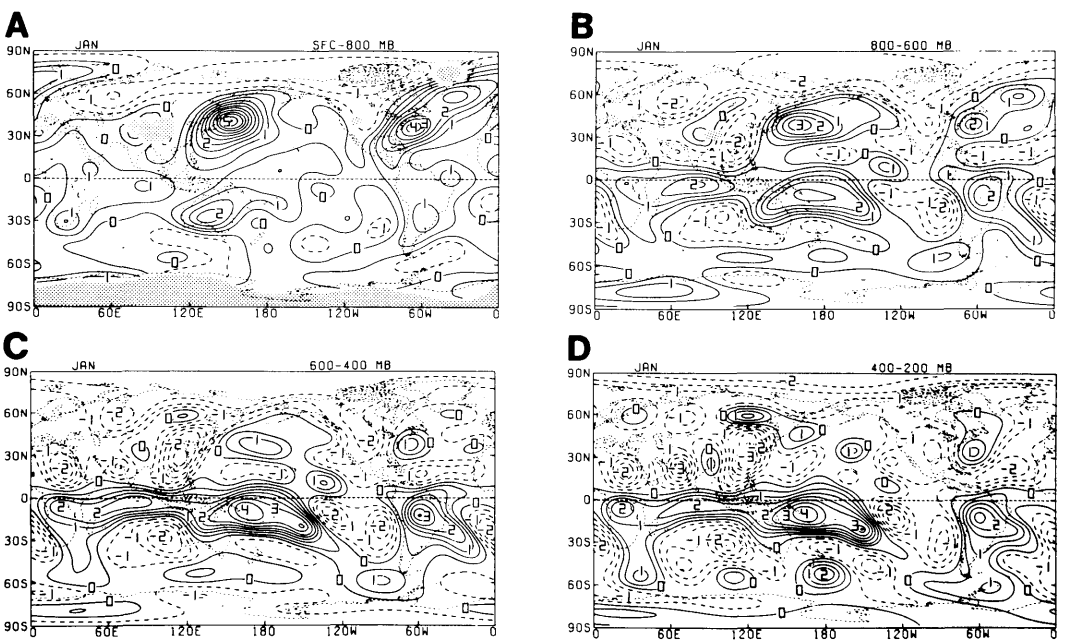

Fig. 6. Mass-weighted layer-averaged heating (°K day^{-1}) estimated for the (A) surface–800 mb, (B) 800–600 mb, (C) 600–400 mb, and (D) 400–200 mb isobaric layers for January 1979. Filtered as in Fig. 2. Contour interval is 0.5°K day^{-1}. Stippling denotes regions where the time-averaged surface pressure is less than the upper level of the layer.

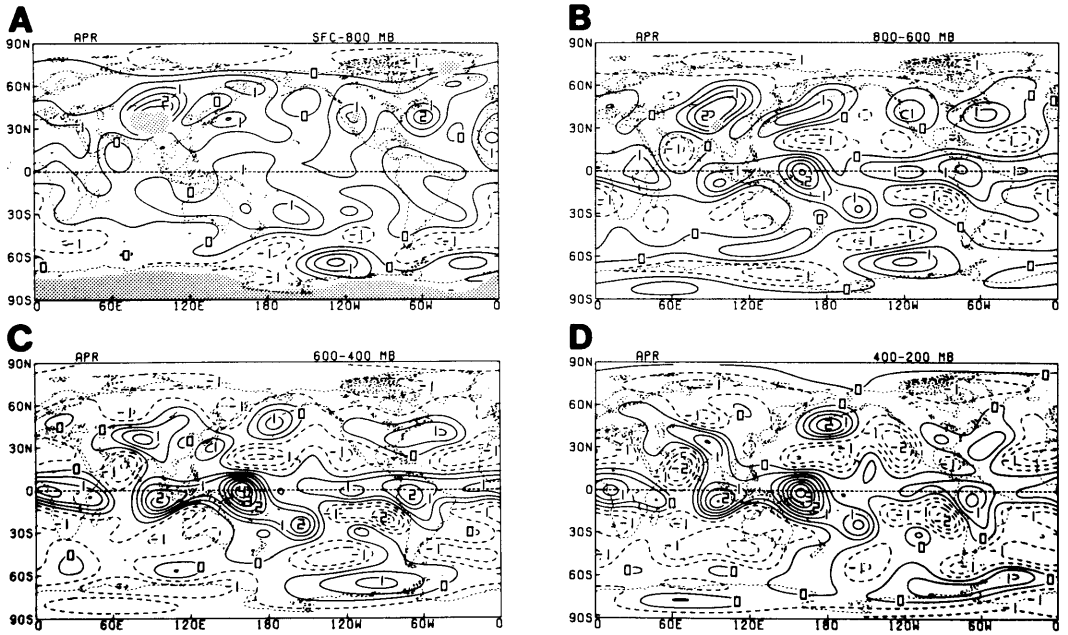

Fig. 7. Same as Fig. 6 except for April 1979.

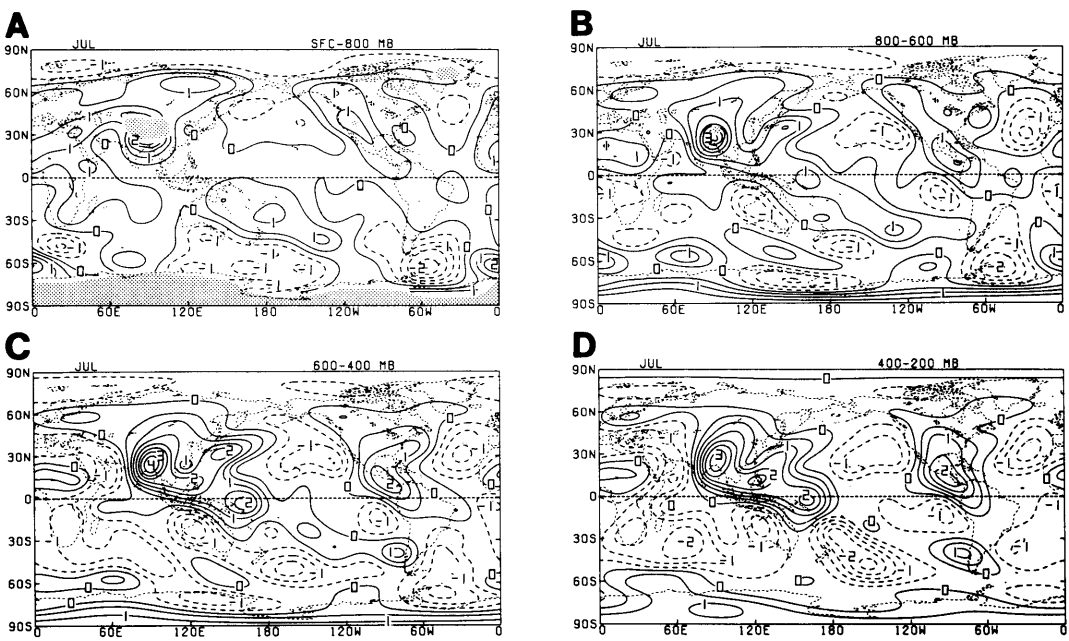

Fig. 8. Same as Fig. 6 except for July 1979.

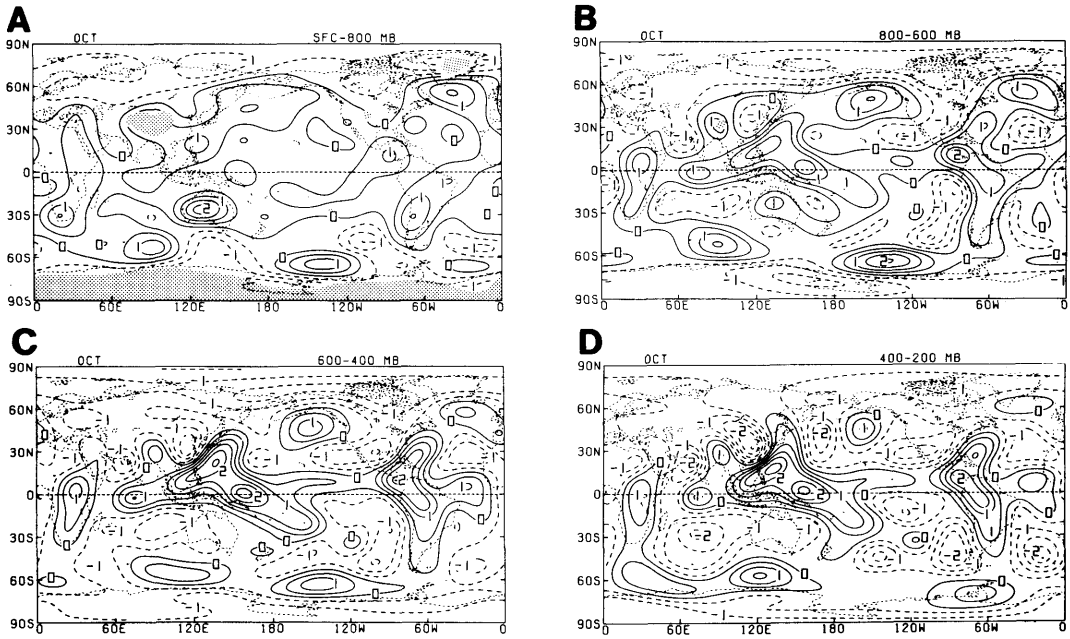

Fig. 9. Same as Fig. 6 except for October 1979.

Pacific to the 600–400 mb layer over the mid-Pacific. The maximum heating over the western North Atlantic remains off the east coast of the United States through all layers.

Tropical latitudes are characterized by strong heating above 800 mb at all longitudes except over the eastern Pacific where cooling prevails. This heating must undoubtedly be associated with deep moist convection. The maximum heating rates in the ITCZ over the equatorial western Pacific and Brazil are located in the upper two layers. The maximum heating over the equatorial western Pacific exceeds 4.0°K day^{-1} in the 400–200 mb layer, while the maximum heating in the ITCZ over the Indian Ocean exceeds 2.0°K day^{-1} in the upper three layers. The maximum heating over Brazil occurs in the 600–400 mb layer.

Cooling rates between 0.5 and 2.0°K day^{-1} occur through the depth of the troposphere over the Eurasian and North American continents and in the upper three layers at nearly all longitudes of the Northern Hemisphere subtropics. Cooling through the upper three layers is indicated within the subtropical anticyclonic circulations to the west of Australia, South America and southern Africa. In each region, the maximum cooling rate exceeds 1.5°K day^{-1}.

Heating occurs through the depth of the troposphere over portions of the western oceans of the Northern Hemisphere in April (Fig. 7). The weaker heating in the sfc–800 mb layer compared to January reflects the reduction in temperature contrast during outbreaks of continental polar air over the warmer ocean. Above 800 mb, the heating is oriented along climatological cyclone tracks of April (Whittaker and Horn, 1982) and reflects latent heat release. The westward extension of heating over the United States in the upper layers also likely reflects latent heating along cyclone tracks.

Heating associated with deep convection within the ITCZ during April is quite evident as nearly all longitudes along the equator experience heating above 800 mb. As in January, the strongest heating occurs above 600 mb with similar heating rates in the upper two layers. Heating rates in the upper two layers exceed 3.5°K day^{-1} over the equator near 160°E and 2.0°K day^{-1} near 100°E in the Indian Ocean.

The cooling over the subtropical North Pacific and North Atlantic in the upper three layers is

consistent with the location of subtropical high pressure systems in these regions. The maximum cooling rates range between 1.0 and 1.5°K day^{-1}. Cooling prevails in the subtropics of the Southern Hemisphere above 800 mb except between 160°E and 140°W, where heating within the SPCZ is indicated in all four layers.

The heating distribution in the sfc–800 mb layer for July (Fig. 8A) shows the expected reversal from the January distribution (Fig. 6A) with heating over the continents and cooling over the eastern oceans in the Northern Hemisphere. The heating over southeast Asia and the equatorial western Pacific, associated with deep moist convection, is maximized above 600 mb. The maximum heating exceeds 4.0°K day^{-1} in the region north of the Bay of Bengal over the foothills of the Himalayas. The SPCZ is well defined by the heating distribution in the lower three layers. In the Western Hemisphere heating in excess of 1.0°K day^{-1} is indicated in the upper three layers over Central America. A maximum greater than 2.0°K day^{-1} occurs in the 400–200 mb layer (Fig. 8D).

Well defined cooling maxima associated with anticyclonic circulations are present in all layers over the eastern North Pacific and Atlantic Oceans. In July these circulations are well established in these regions. Cooling occurs through the depth of the troposphere over most of the extratropical latitudes of the Southern Hemisphere.

In October, the heating in tropical latitudes is relatively uniform in the two layers above 600 mb (Figs. 9C–D). Axes of strong heating extend from regions of tropical convection over the equatorial western Pacific and Central America along the east coasts of Asia and North America. The heating maxima over the Gulf of Alaska and southeast of Greenland correspond with areas of maximum cyclone frequency in October for the 20-year period from 1958–1977 (Whittaker and Horn, 1982).

Cooling ranging between 0.5 and 2.0°K day^{-1} is indicated over Northern Hemisphere continents in the layers above 800 mb. Above 800 mb, cooling within anticyclonic circulations over the eastern oceans of the Northern Hemisphere and to the west of Africa, Australia and South America ranges between 0.5 and 2.0°K day^{-1}. These cooling rates are consistent with the rates found within oceanic anticyclonic circulations for the other three months.

5. Summary and conclusions

A detailed knowledge of the spatial and temporal distributions of atmospheric heat sources and sinks is ultimately important for understanding the structure and evolution of atmospheric circulation. Besides the need to resolve the horizontal distribution of heat sources and sinks, results from simple models have demonstrated the sensitivity of circulation to the vertical structure of heating in both tropical (Hartmann et al., 1984) and extratropical (Smagorinsky, 1953; Trenberth, 1983) latitudes.

The main objective of this paper was to examine the large-scale three-dimensional distribution of atmospheric heating and its temporal evolution as determined from the ECMWF GWE Level IIIb analyses. Results were presented for January, April, July and October 1979. Global distributions of vertically averaged heating were presented to illustrate the seasonal evolution of the planetary pattern. Profiles from various geographical locations were presented to indicate the seasonal evolution of the vertical structure of atmospheric heating in different climatological regimes. A global perspective of the vertical structure of atmospheric heating was depicted in the layer-averaged results presented for each of the four months. Our preliminary evaluation based on climatological and physical considerations indicates that the quality of the GWE analyses appears to render credible estimates of heating. While only information on the total heating can be obtained from the method of calculation utilized, the changing relative importance of sensible, latent and radiational heating components is evident from physical and climatological considerations.

Major features of the vertically averaged heating distributions include the heating within the regions of deep convection over Brazil, equatorial Africa, the ITCZ, the Asian monsoon circulation, and in the oceanic cylone tracks over the western oceans of the Northern Hemisphere. Heating over the oceans and cooling over the continents prevails in the winter while the reverse is true in the summer. This relation is particularly

pronounced in the Northern Hemisphere. Cooling dominates in polar regions and within anticyclonic circulations of the subtropics.

In accord with the changing seasons, the heating within the ITCZ and the Asian monsoon circulation migrates from one hemisphere to the other. During January, the maximum heating associated with the Asian monsoon assumes its southern- and eastern-most position being located south of the equator near 165°E. In July, the maximum heating assumes its northern- and western-most position just north of the Bay of Bengal over the foothills of the Himalayas, while intermediate positions occur in April and October. Similarly, regions of heating over Africa and the Americas move in concert with the sun from one hemisphere to the other. Heating over the western oceans of the Northern Hemisphere with the maximum intensity occurring during January is a persistent feature in all four months studied.

Many interesting features are evident from examination of the vertical profiles of heating. Within the deep moist convection associated with both the summer and winter Asian monsoon circulations, the maximum heating occurs in the upper troposphere near 400 mb. The profiles in the present study are in agreement with estimates from previous investigations for corresponding regions. The seasonality of the Indian monsoon is reflected in the profiles over central India. These profiles show relatively strong heating through the depth of the troposphere in July which is indicative of latent heat release within deep convection of the summer monsoon. The cooling which occurs in the middle and upper troposphere in the other seasons is in all probability due to radiational cooling.

Profiles from desert regions over the Sahara and Australia show a transition from low tropospheric heating to upper level cooling, apparently reflecting the dominance of sensible heating near the surface and radiational cooling aloft. Over the storm tracks off the Asian and North American coasts, the importance of both sensible and latent heating can be discerned as these regions display strong low level heating and moderate heating through much of the middle and upper troposphere. However, the vertical structures of the time-averaged heating along these two storm tracks over the western North Pacific and North Atlantic are somewhat different. The results show that both the upper and lower level heating over the North Atlantic are maximized at the same location between the latitudes of 30° and 40°N. Over the western North Pacific, the maximum heating is displaced upward starting from the intense low level heating over the Kuroshio Current at the western boundary to strong latent heating in the mid Pacific.

The cooling over continental regions of the Northern Hemisphere during winter ranges between 0.5 and 1.5°K day^{-1} throughout much of the troposphere. Similar cooling rates occur within oceanic anticyclonic circulations over the eastern oceans of both hemispheres. These profiles are comparable with zonal mean radiative cooling rates estimated by Dopplick (1972).

The accuracy of the heating estimates presented depends on many factors. The GWE Level III data sets are the products of complex assimilation models. Each assimilation system used to produce GWE Level III analyses has its own characteristics which may impact results derived from the data especially in data sparse regions. Consequently, the heating estimates determined from Level III data depend on the quality of the observations, the assimilation model and the diagnostic method utilized. Lorenc and Swinbank (1984), Boer (1986) and Holopainen and Fortelius (1986) provide comparisons of heating estimates computed from various GWE data sets for corresponding time periods.

In the present study, the interpolation of the ECMWF Level III data to form an isentropic data set, the creation of surface data and the interpolation of heating rates back to isobaric levels for purposes of displaying the vertical variation of heating introduce some uncertainty. The lack of the information on the diabatic mass flux at the uppermost level of the analysis and the method of adjustment employed in estimating the diabatic mass flux also are sources of errors in the computation. In addition, most of the stratosphere is excluded from consideration in this investigation due to certain questionable features. Improving the stratospheric analyses is one of the objectives of the GWE re-analysis effort (National Research Council, 1985). Inclusion of the stratospheric information from the re-analyzed Level III data sets may lead to some refinement of heating estimates.

The apparent spatial and temporal continuity of the heating distributions presented and their consistency with known circulation features suggests that a realistic three-dimensional structure of the thermal forcing of the global circulation emerges. Similar studies utilizing other GWE data sets from past, current or future Level III assimilations, as well as data sets from other years should be performed to gain understanding of the link of teleconnections and climatic anomalies with the global distribution of differential heating and thermally forced monsoonal circulations. Investigations into the global water vapor and radiative balance of the atmosphere will also lend insight into the roles played by the individual components of heating.

6. Acknowledgements

This research was sponsored by the National Science Foundation under Grant ATM-8517273 and by the National Aeronautics and Space Administration under Grant NAG5-81. Typing of the manuscript by Judy Mohr and preparation of the figures by Christine Johnson and Kim Koepsel are greatly appreciated.

7. Appendix

Adjustment of the diabatic mass flux

The adjustment for diabatic mass flux is based on the constraint that the sum of the vertically integrated mass tendency and mass divergence must be consistent with boundary values of the diabatic mass flux. The vertical integral of the isentropic mass continuity equation is expressed by

$$(\rho J_\theta \dot{\theta})|_{\theta_s} = \int_{\theta_s}^{\theta_T} \left[\frac{\hat{c}}{\hat{c}t_\theta} (\rho J_\theta) + \nabla_\theta \cdot (\rho J_\theta \underline{U}) \right] \mathrm{d}\theta, \quad \text{(A1)}$$

where θ_T is the potential temperature of the upper surface of the region of integration and θ_s is the surface potential temperature. The diabatic mass flux at θ_T is assumed to vanish. By virtue of the systematic errors associated with biases in the estimates of the tendency and the divergence of the horizontal transport, the computed diabatic mass flux at the earth's surface from (A1) will not be consistent with an estimate of the diabatic mass flux at the earth's surface given by the temporal variation of the surface distribution of potential temperature.

The temporal variation of the surface potential temperature $\theta_s(\lambda, \phi, t)$ from the chain rule is expressed by

$$\dot{\theta}_s(\lambda, \phi, t) = \frac{\hat{c}\theta_s}{\hat{c}t_\theta} + \underline{U}_s \cdot \nabla_\theta \theta_s. \quad \text{(A2)}$$

In view of the quasi-Lagrangian nature of the earth's surface with respect to isentropic coordinates and in view of the requirement that the diabatic mass flux from (A1) must be consistent with the change of potential temperature at the earth's surface, the true value $(\rho J_\theta \dot{\theta})|^*_{\theta_s}$ is assumed to be given by

$$\rho J_\theta \dot{\theta}|^*_{\theta_s} = \rho J_\theta \dot{\theta}_s = \rho J_\theta \left(\frac{\hat{c}\theta_s}{\hat{c}t_\theta} + \underline{U}_s \cdot \nabla_\theta \theta_s \right). \quad \text{(A3)}$$

The difference between (A1) and (A3) represents the integrated systematic error (δ) given by

$$\delta = (\rho J_\theta \dot{\theta})|_{\theta_s} - (\rho J_\theta \dot{\theta})|^*_{\theta_s}. \quad \text{(A4)}$$

Let $\hat{\delta}$ represent the error per unit mass within the atmospheric column

$$\hat{\delta} = \delta \Big/ \int_{\theta_s}^{\theta_T} \rho J_\theta \mathrm{d}\theta = -g\delta/[p(\theta_T) - p(\theta_s)]. \quad \text{(A5)}$$

With this definition, the adjusted diabatic mass flux at an isentropic level is defined by

$$(\rho J_\theta \dot{\theta})' = \int_{\theta}^{\theta_T} \left[\frac{\hat{c}}{\hat{c}t_\theta} (\rho J_\theta) + \nabla_\theta \cdot (\rho J_\theta \underline{U}) - \rho J_\theta \hat{\delta} \right] \mathrm{d}\theta. \quad \text{(A6)}$$

In this method the integrated error is distributed through the atmospheric column in proportion to the mass within an isentropic layer.

REFERENCES

Bengtsson, L., Kanamitsu, M., Kållberg, P. and Uppala, S. 1982. FGGE 4-dimensional data assimilation at ECMWF. *Bull. Amer. Meteor. Soc. 63*, 29–43.

Boer, G. J. 1986. A comparison of mass and energy budgets from two FGGE datasets and a GCM. *Mon. Wea. Rev. 114*, 885–902.

Boyle, J. S. and Chen, T.-J. 1987. Synoptic aspects of the east Asian monsoon. In: *Monsoon Meteorology* (eds. C.-P. Chang and T. N. Krishnamurti). New York: Oxford University Press, 125–160.

Brown, J. A. 1964. A diagnostic study of the tropospheric diabatic heating and the generation of available potential energy. *Tellus 16*, 371–388.

Budyko, M. I. 1963. *Atlas of the heat balance of the earth*. Moscow: Gidrometoizdazt, 69 pp.

Chen, T.-C. and Baker, W. E. 1986. Global diabatic heating during FGGE SOP-1 and SOP-2. *Mon. Wea. Rev. 114*, 2578–2589.

Chen, T.-C., Chang, C. B. and Perkey, D. J. 1985. Synoptic study of a medium-scale oceanic cyclone during AMTEX, 75. *Mon. Wea. Rev. 113*, 349–361.

Chen, S.-J. and Dell'osso, L. 1987. A numerical case study of east Asian coastal cyclogenesis. *Mon. Wea. Rev. 115*, 477–487.

Davidson, N. W. 1984. Short-term fluctuations in the Australian Monsoon during winter Monex. *Mon. Wea. Rev. 112*, 1697–1708.

Dopplick, T. G. 1972. Radiative heating of the global atmosphere. *J. Atmos. Sci. 29*, 1278–1294.

Geller, M. A. and Avery, S. K. 1978. Northern Hemisphere distributions of diabatic heating in the troposphere derived from general circulation data. *Mon. Wea. Rev. 106*, 629–636.

Gerrity, J. P. 1977. The LFM model–1976: a documentation. NOAA Technical Memorandum, *NWS NMC 60*, 68 pp.

Gruber, A., Varnadore, M., Arkin, P. A. and Winston, J. S. 1986. Monthly and seasonal mean outgoing longwave radiation and anomalies. NOAA Tech. Rept. NESDIS 26, U.S. Dept. of Commerce, NOAA/NESDIS, Washington, D.C.

Hantel, M. and Baader, H.-R. 1978. Diabatic heating climatology of the zonal atmosphere. *J. Atmos. Sci. 35*, 1180–1189.

Hartmann, D. L., Hendon, H. H. and Houze, R. A. 1984. Some implications of the mesoscale circulations in tropical cloud clusters for large-scale dynamics and climate. *J. Atmos. Sci. 41*, 113–121.

Heddinghaus, T. R. and Krueger, A. F. 1981. Annual and interannual variations in outgoing longwave radiation over the tropics. *Mon. Wea. Rev. 109*, 1208–1218.

Holopainen, E. and Fortelius, C. 1986. Accuracy of estimates of atmospheric large-scale energy flux divergence. *Mon. Wea. Rev. 114*, 1910–1921.

Houze, R. A. 1982. Cloud clusters and large-scale vertical motions in the tropics. *J. Meteor. Soc. Japan 60*, 396–410.

Jaeger, L. 1976. "Monatskarten des Niederschlags für die ganze Erde" ["Monthly precipitation maps for the entire earth"]. *Ber. Dtsch. Wetterdienstes 18*, No. 139.

Johnson, D. R. 1980. A generalized transport equation for use with meteorological coordinate systems. *Mon. Wea. Rev. 108*, 733–745.

Johnson, D. R. 1985. The global circulation during the FGGE year: on the balance of mass, energy, and angular momentum within isentropic and isobaric coordinates as revealed by different FGGE data sets. Presented at the Global Weather Experiment Scientic Seminar, Helsinki, Finland, 29–31 August, 1984. *GARP Special No. 42, II*, 28–40.

Johnson, D. R. and Wei, M.-Y. 1985. The planetary distribution of heat sources and sinks during FGGE. *Proceedings of the First National Workshop on the Global Weather Experiment: Current Achievements and Future Directions*, Vol. 2, Part I, 299–316. Washington, D.C.: National Academy of Sciences.

Johnson, D. R., Townsend, R. D. and Wei, M.-Y. 1985. The thermally coupled response of the planetary scale circulation to the global distribution of heat sources and sinks. *Tellus 37A*, 106–125.

Johnson, D. R., Yanai, M. and Schaack, T. K. 1987. Global and regional distributions of atmospheric heat sources and sinks during the GWE. In: *Monsoon meteorology* (eds. C.-P. Chang and T. N. Krishnamurti). New York: Oxford University Press, 271–297.

Johnson, R. H. and Young, G. S. 1983. Heat and moisture budgets of tropical mesoscale anvil clouds. *J. Atmos. Sci. 40*, 2138–2147.

Julian, P. R. 1983. Comments on the ECMWF IIIb analysis data set. U.S. Committee for GARP, *Global Weather Experiment Newsletter, No. 1*, 15–17.

Kasahara, A. and Mizzi, A. P. 1985. Preliminary evaluation of diabatic heating distribution from FGGE Level IIIb analysis data. *Proceedings of the First National Workshop on the Global Weather Experiment: Current Achievements and Future Directions*, Vol. 2, Part I, 317–329. Washington, D.C.: National Academy of Sciences.

Kasahara, A., Mizzi, A. P. and Mohanty, U. C. 1987. Comparison of global diabatic heating rates from FGGE Level IIIb analyses with satellite radiation imagery data. *Mon. Wea. Rev. 115*, 2904–2935.

Lau, N.-C. 1979. The observed structure of tropospheric stationary waves and the local balances of vorticity and heat. *J. Atmos. Sci. 36*, 996–1016.

Lorenc, A. C. and Swinbank, R. 1984. On the accuracy of general circulation statistics calculated from FGGE data—a comparison of results from two sets of analyses. *Quart. J. Roy. Meteor. Soc. 110*, 915–942.

Luo, H. and Yanai, M. 1984. The large-scale circulation and heat sources over the Tibetan Plateau and surrounding areas during the early summer of 1979. Part II: Heat and moisture budgets. *Mon. Wea. Rev. 112*, 966–989.

Masuda, K. 1983. Dynamical estimation of atmospheric diabatic heating over the Northern Hemisphere in winter. *J. Meteor. Soc. Japan 61*, 449–454.

Masuda, K. 1984. Diabatic heating during the FGGE: a preliminary report. *J. Meteor. Soc. Japan 62*, 702–708.

Miller, B. L. and Vincent, D. G. 1987. Convective heating and precipitation estimates for the tropical South Pacific during FGGE, 10–18 January 1979. *Quart. J. Roy. Meteor. Soc. 113*, 189–212.

Murakami, M. 1983. Analysis of the deep convective activity over the Western Pacific and Southeast Asia. Part I: Diurnal variation. *J. Meteor. Soc. Japan 61*, 60–75.

National Research Council 1985. *Proceedings of the First National Workshop on the Global Weather Experiment*, Vols. I and II. Board on Atmospheric Sciences and Climate, National Academy Press, Washington, D.C., Vol. I, 75 pp., Vol., II, 809 pp.

Newell, R. E., Vincent, D. G., Dopplick, T. G., Ferruzza, D. and Kidson, J. W. 1969. The energy balance of the global atmosphere. In: *The global circulation of the atmosphere* (ed. G. A. Corby). Roy. Meteor. Soc., 42–90.

Newell, R. E., Kidson, J. W., Vincent, D. G. and Boer, G. J. 1974. *The general circulation of the tropical atmosphere and interactions with extratropical latitudes*, Vol. 2. The MIT Press, 371 pp.

Nitta, T. 1983. Observational study of heat sources over the eastern Tibetan Plateau during the summer monsoon. *J. Meteor. Soc. Japan 61*, 590–605.

Nitta, T. and Yamamoto, J. 1974. On the observational characteristics of intermediate scale disturbances generated near Japan and the vicinity. *J. Meteor. Soc. Japan 52*, 11–31.

Otto-Bliesner, B. L. and Johnson, D. R. 1982. Thermally-forced mean mass circulations in the Northern Hemisphere. *Mon. Wea. Rev. 110*, 916–932.

Physick, W. L. 1981. Winter depression tracks and climatological jet streams in the Southern Hemisphere during the FGGE year. *Quart. J. Roy. Meteor. Soc. 107*, 883–898.

Reed, R. J. and Recker, E. E. 1971. Structure and properties of synoptic-scale wave disturbances in the equatorial western Pacific. *J. Atmos. Sci. 28*, 1117–1133.

Sardeshmukh, P. D. 1984. *The global circulation of the atmosphere during January–November 1979 based upon ECMWF analyses*. Department of Meteorology, University of Reading, England, 144 pp.

Savijärvi, H. I. 1988. Global energy and moisture budgets from rawinsonde data. *Mon. Wea. Rev. 116*, 417–430.

Schmidt, P. J. and Johnson, D. R. 1972. Use of approximating polynomials to estimate profiles of wind, divergence and vertical motion. *Mon. Wea. Rev. 100*, 345–353.

Staff members of the Section of Synoptic and Dynamic Meteorology, Inst. of Geophys. and Meteor., Acad. Sin., 1958. On the general circulation over eastern Asia (II). *Tellus 10*, 58–75.

Smagorinsky, J. 1953. The dynamical influence of large-scale heat sources and sinks on the quasi-stationary mean motions of the atmosphere. *Quart. J. Roy. Meteor. Soc. 79*, 342–366.

Sumi, A. and Murakami, T. 1981. Large-scale aspects of the 1978–79 winter circulation over the greater WMONEX region. Part I: Monthly and season mean fields. *J. Meteor. Soc. Japan 59*, 625–645.

Susskind, J. and Kalnay, E. 1985. Remote sensing of atmospheric and surface parameters from HIRS2/MSU on TIROS-N. *Proceedings of the First National Workshop on the Global Weather Experiment: Current Achievements and Future Direction*, Vol. 2, Part I, 361–384. Washington, D.C.: National Academy of Sciences.

Trenberth, K. E. 1983. Interactions between orographically and thermally forced planetary waves. *J. Atmos. Sci. 40*, 1126–1152.

Webster, P., Chou, L. and Lau, K. M. 1977. Mechanisms effecting the state of the planetary scale monsoon. *Pure Appl. Geophys. 115*, 1463–1491.

Wei, M.-Y., Johnson, D. R. and Townsend, R. D. 1983. Seasonal distributions of diabatic heating during the First GARP Global Experiment. *Tellus 35A*, 241–255.

Wiin-Nielsen, A. and Brown, Jr., J. A. 1962. On diagnostic computations of atmospheric heat sources and sinks and the generation of available potential energy. *Proc. of the Int. Symp. on Numerical Weather Prediction*, Meteor. Soc. of Japan, Tokyo, 519–613.

Whittaker, L. M. and Horn, L. H. 1982. *Atlas of Northern Hemisphere extratropical cyclone activity, 1958–1977*. Department of Meteorology, University of Wisconsin, Madison, Wisconsin, 65 pp.

Yanai, M., Esbensen, S. and Chu, J.-H. 1973. Determination of bulk properties of tropical cloud clusters from large-scale heat and moisture budgets. *J. Atmos. Sci. 30*, 611–627.

Yeh, T.-C. and Gao, Y.-X. et al. 1979. *The Meteorology of the Qinghai-Xizang (Tibet) Plateau*. Beijing: Science Press, 278 pp (in Chinese).

Zillman, J. W. and Johnson, D. R. 1985. Thermally-forced mean mass circulations in the Southern Hemisphere. *Tellus 37A*, 56–76.